1. INTRODUCTION

Small GTPases H-Ras, K-Ras, and N-Ras, collectively called Ras, function as a molecular switch by cycling between GTP-bound active and GDP-bound inactive forms (Ras·GTP and Ras·GDP, respectively) in a variety of intracellular signaling pathways controlling cell growth, differentiation, and apoptosis [1]. Ras·GTP binds directly and activates downstream effectors such as Raf kinases (c-Raf-1, B-Raf, and A-Raf, collectively called Raf), phosphoinositide 3-kinases (PI3Ks), Ral guanine nucleotide dissociation stimulator (RalGDS) family proteins, and phospholipase Cε. Raf and PI3Ks induce activation of downstream kinase cascades MEK/ERK and PDK/Akt, respectively, while RalGDS activates small GTPase RalA. Not only Raf but also PI3Ks and RalGDS are implicated in malignant transformation. Interconversion between the two forms is reciprocally catalyzed by guanine nucleotide exchange factors (GEFs) and GTPase-activating proteins (GAPs) [2]. In particular, GEFs such as Son-of-sevenless (Sos) mediate various upstream signals to induce formation of Ras·GTP. The GTP/GDP exchange induces allosteric conformational changes in two flexible regions, termed switch I (residues 32–38) and switch II (residues 60–75), both of which constitute a principal interface for effector recognition [2]. Oncogenic potential of Ras is enhanced by point mutations at particular residues such as Gly12 and Gln61, which not only impair the intrinsic GTPase activity but also render Ras insensitive to the GAP action, resulting in the constitutive activation of the downstream effectors [1]. Such mutational activation of Ras is observed in a variety of human cancers at an overall frequency of 15–20%, and this frequency goes up to 60–90% and 30–50% in pancreatic and colorectal cancers, respectively [1,3,4]. Cancer cells with activated oncogenes such as *ras* are known to exhibit a phenomenon called "oncogene addiction," where their survival becomes dependent on the activated oncogene functions [3]. In such a case, inhibition of the activated Ras function causes the reversal of transformed phenotypes of cancer cells, eventually leading to cell death and tumor regression [4,5]. Although these data feature Ras as one of the most promising target for anticancer drug development, there is no effective molecular targeted therapy for Ras at present now that once highly anticipated farnesyl transferase inhibitors, which block posttranslational farnesylation of Ras necessary for membrane targeting, have failed in clinical trials [1,6]. Farnesylthiosalicylic acids, *S*-farnesyl cysteine mimetics which inhibit binding of Ras to the

Ras-escort proteins in the plasma membrane, have also been developed but their antitumor activity remains unclear [7]. However, in these 2 years, there have been significant advances in developing new strategies for Ras inhibitor discovery, which will be discussed in Section 7.

In this chapter, we review our strategy for Ras inhibitor development, where structural information on drug-accepting pockets found in a novel crystal structure of Ras·GTP is effectively utilized for structure-based drug design (SBDD) of a novel class of small-molecule Ras inhibitors, which block binding of Ras·GTP to multiple effector molecules and exhibit antitumor activity toward a xenograft of human colon carcinoma cells carrying the activated K-*rasG12V* gene.

2. DISCOVERY OF SURFACE POCKETS IN NOVEL CRYSTAL STRUCTURES OF Ras·GTP

Successful discoveries by using SBDD of small-molecule drugs, such as anti-HIV and anti-influenza drugs, have boosted hopes for the application of this approach to anticancer drug development targeting the oncogene products. However, Ras have been presumed to be refractory to this approach owing to the absence of "druggable" surface pockets in their crystal structures determined in as early as the late 1980s [8]. It is not until the year of 2005 that such a drug-accepting surface pocket was recognized by us in the crystal structure of a Ras homologue M-Ras in complex with a nonhydrolyzable GTP analogue guanosine 5′-(β,γ-imido)triphosphate (GppNHp), which corresponded to a novel conformation, called state 1, undergoing dynamic equilibrium with the previously known conformation, called state 2 [9–11] (see Section 8 for the details of the conformational dynamics of Ras·GTP). However, crystallization and structure determination of the state 1 conformations of wild-type H-Ras, K-Ras, and N-Ras were not technically feasible at that time. This prompted us to use the surface pocket structure of M-Ras·GppNHp state 1 as a target model for SBDD of small-molecule compounds that fit into the pocket and potentially interfere with the Ras functions. We thought that this was reasonable because M-Ras shares identical amino acid sequence in the switch I region with the three Ras oncoproteins and is capable of interacting with some of the Ras–effector molecules such as c-Raf-1. Also, the surface pocket of M-Ras·GppNHp is located in close proximity to the two switch regions, which form the major effector-binding interface, suggesting that compounds that fit into the pocket may interfere with the effector binding by steric hindrance.

Actually, the crystal structure of M-Ras·GppNHp had serious problems for use in *in silico* docking simulation because its resolution was as low as 2.2 Å and the electron density for the five residues in switch II, forming an edge of the surface pocket, was missing [9]. Thus, we made an initial attempt to conduct an *in silico* docking screen of a virtual compound library based on a predicted model structure of a pocket reconstructed from the switch I structure of M-Ras·GppNHp and the remaining portion of the H-RasQ61L·GppNHp crystal structure (PDB ID: 721P), which turned out to be unsuccessful in finding compounds with the activity to inhibit Ras–Raf binding *in vitro*. In the mean time, we determined a high-resolution crystal structure of the state 1 conformation by using an M-RasP40D mutant carrying an H-Ras-type amino acid substitution immediately preceding switch I for analysis of the state transition mechanisms in 2006 [10], which gave us complete structure of the surface pocket with a high resolution of 1.35 Å (Fig. 1.1A). This prompted us to conduct an *in silico* docking screen targeting the pocket structure of M-RasP40D·GppNHp.

M-RasP40D·GppNHp (PDB ID: 3KKP) possesses a relatively large surface pocket surrounded by the two switch regions and the nucleotide (Fig. 1.1B). The pocket consists of two parts: one is a hydrophilic part (hereafter called the hydrophilic pocket) located in close proximity to GppNHp, which is composed of negatively charged residues such as Glu47, Asp48, and Asp67, and the other is a hydrophobic part (hereafter called the hydrophobic pocket), which consists of Leu66, Met77, and Tyr81 on its surface and is partly edged by charged residues such as Lys15 and Asp67. (Note that M-Ras is 10-amino acid longer than Ras oncoproteins at its N terminus.) These structural features convinced us to set the pharmacophore for the screening to the charged residues, such as Asp67 (corresponding to Asp57 in Ras) located at the bottom center of the hydrophilic pocket, rather than the hydrophobic residues in order to secure the binding specificity and energy.

As for the crystal structure of H-Ras·GppNHp state 1, we succeeded in its determination by using a mutant H-RasT35S in complex with GppNHp, which predominantly assumes the state 1 conformation [10]. The solution structure of H-Ras·GppNHp state 1 was also determined by multi-dimensional heteronuclear analysis of H-RasT35S·GppNHp [11]. Moreover, the state 1 crystal structures of the GppNHp-bound forms of H-Ras wild type and its activated mutants H-RasG12V and H-RasQ61L were successfully determined by using the cross-seeding method, where their crystals were grown on the seeds of the microcrystals of

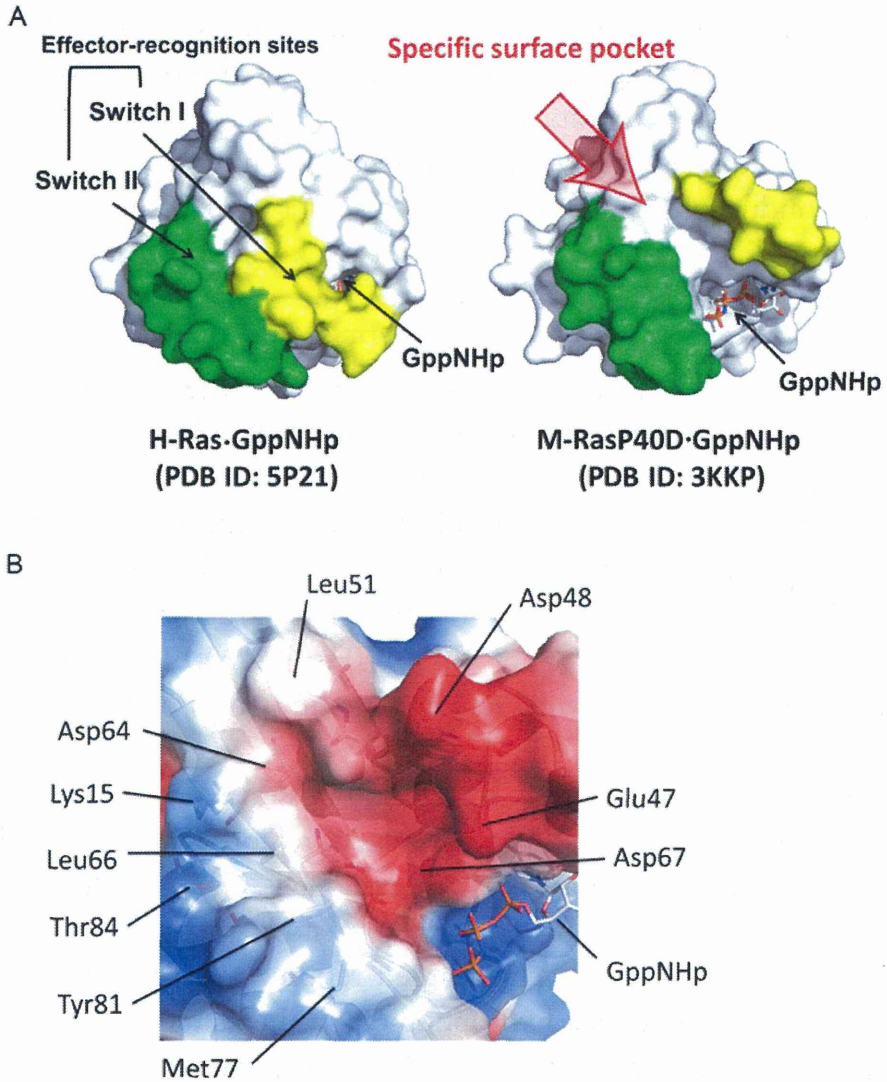

Figure 1.1 A novel crystal structure of Ras·GTP and an enlargement of its surface pocket. (A) A novel crystal structure solved with M-RasP40D·GppNHp (right) possessed a surface pocket surrounded by switch I, switch II, and guanine nucleotide while such a pocket did not exist in the previously determined crystal structures of H-Ras·GppNHp. (B) A close-up view of the surface pocket of M-Ras·GppNHp. The positive and negative charges on the protein surface are shown in blue and red, respectively.

H-RasT35S·GppNHp [12]. All of these state 1 crystal structures possessed surface pockets similar to that of M-RasP40D·GppNHp and could be used for new rounds of *in silico* screening.

3. DISCOVERY OF THE Kobe0065-FAMILY COMPOUNDS BY *IN SILICO* SCREENING

An *in silico* docking screen was conducted by targeting the surface pocket of M-RasP40D·GppNHp (PDB ID: 3KKP) as summarized in

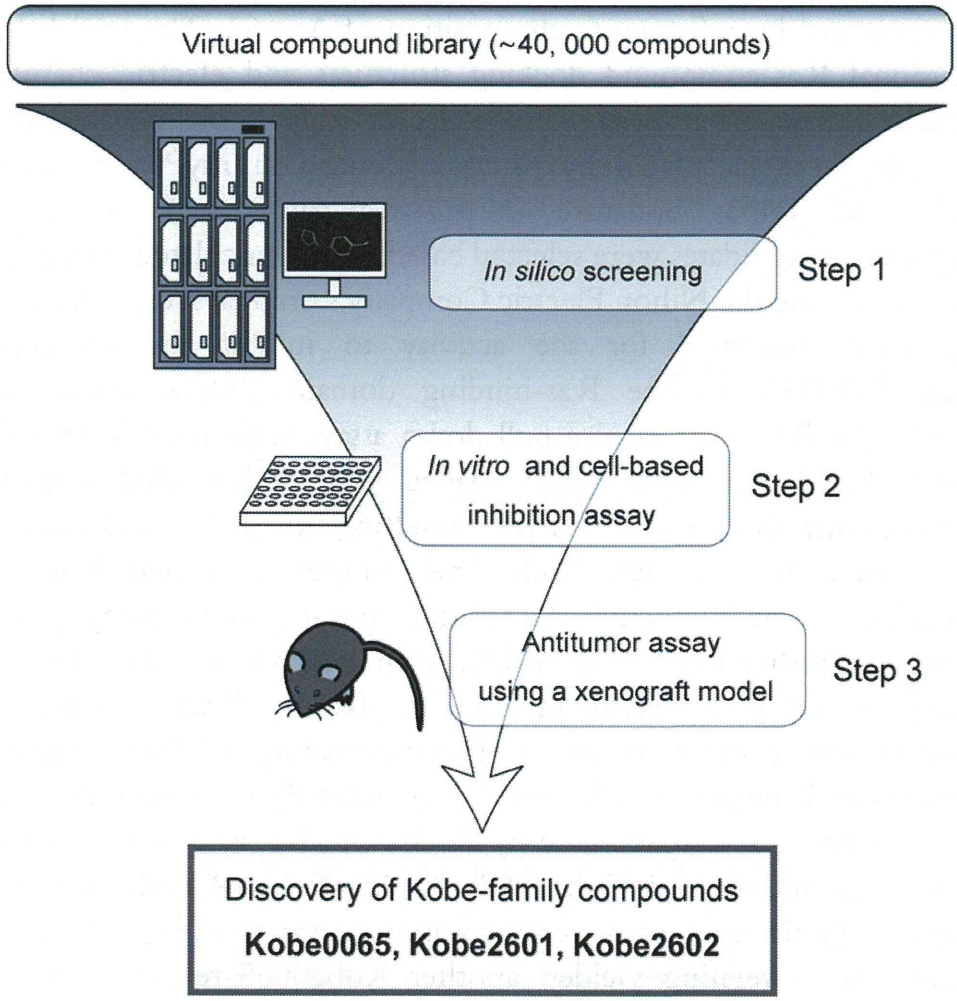

Figure 1.2 Strategy for the development of Ras inhibitors used in this study. Step 1: screening for candidate compounds by *in silico* docking simulation targeting the surface pocket of M-RasP40D·GppNHp. Step 2: assays for the inhibitory activities of the selected compounds toward *in vitro* Ras–Raf binding and proliferation of cancer cell lines carrying the activated *ras* oncogenes. Step 3: assays for the antitumor activity of the compounds on a xenograft of human colon cancer cells carrying the K-*rasG12V* oncogene.

Fig. 1.2. We applied the molecular mechanics Poisson–Boltzman surface area method with an Assisted Model Building and Energy Refinement 96 force field, where solvent effect on binding free energy was introduced upon simulation [13]. A commercially available virtual library from Namiki Shoji Co., Ltd. (http://www.namiki-s.co.jp) containing 40,882 compounds was initially filtered by application of "Lipinski's rule of five" for selection of drug-like compounds, yielding 40,307 compounds. Upon docking simulation, the target pocket of M-RasP40D·GppNHp was specified by amino acid residues located within a 6.5-Å distance from the probe points, which

were generated by referring to the position of Asp-67. The initial three-dimensional Ras-compound docking structures and electric charges of the molecules in the presence or absence of water molecules around an Mg^{2+} ion were calculated by using Sievegene in myPresto Software [14,15] and Tripos Software (http://www.tripos.com), respectively. Ninety-seven candidates were selected based on the calculated docking free energy values and the Nihon Electric Company's original scoring functions. They were examined for the activity to inhibit the binding of M-RasP40D·GTP to the Ras-binding domain (RBD, amino acids 50–131) of c-Raf-1 by *in vitro* pull-down assays with resin-immobilized c-Raf-1 RBD of M-RasP40D loaded with ^{35}S-labeled guanosine 5′-3-*O*-(thio)triphosphate (GTPγS), resulting in the identification of six positives. Among them, only one compound named Kobe0065, *N*-(3-chloro-4-methylphenyl)-2-{2,6-dinitro-4-(trifluoromethyl)phenyl} hydrazinecarbothioamide (Fig. 1.3A), exhibited activity to inhibit the binding between H-Ras·GTP and c-Raf-1 RBD. Subsequent computer-assisted similarity search of approximately 160,000 compounds based on the Tanimoto coefficient [17] selected 273 compounds, among which one positive was identified by the *in vitro* H-Ras–Raf-binding inhibition assays and named Kobe2602, 2-{2,6-dinitro-4-(trifluoromethyl) phenyl}-*N*-(4-fluorophenyl)hydrazinecarbothioamide (Fig. 1.3A). In addition, this screening yielded another Kobe0065-related compound named Kobe2601, 2-(2,4-dinitrophenyl)-*N*-(4-fluorophenyl)hydrazine-carbothioamide, which showed much weaker inhibition activity.

4. INHIBITION OF Ras FUNCTIONS BY THE Kobe0065-FAMILY COMPOUNDS

4.1. Inhibition of Ras–Effector interaction

Kinetic analyses of the Ras–Raf-binding inhibition reactions by the compounds showed that Kobe0065 and Kobe2602 competitively inhibit the binding of H-Ras·GTP to c-Raf-1 RBD with K_i values of 46 ± 13 and 149 ± 55 μM, respectively. At the cellular level, these two compounds, added to the culture medium at up to 20 μM, effectively reduced the amount of c-Raf-1 associated with H-RasG12V in NIH3T3 cells in a dose-dependent manner, indicating the inhibition of the Ras activity (Fig. 1.3B). By contrast, sorafenib [18], an inhibitor of multiple protein kinases including Raf, failed to show this activity (data not shown). A similar effect was observed with NIH3T3 cells overexpressing

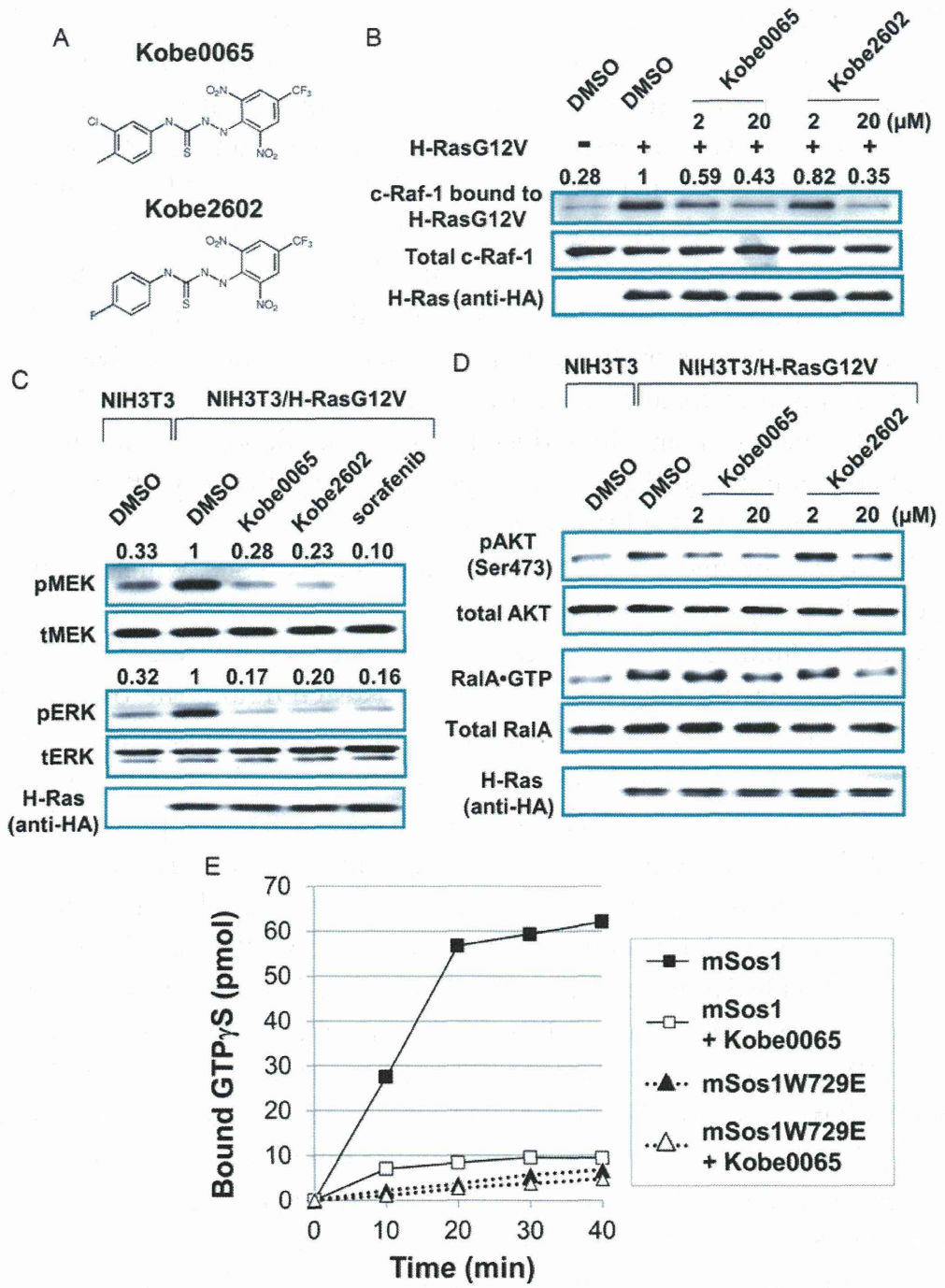

Figure 1.3 Inhibitory effects of the Kobe0065-family compounds on Ras–effector interaction. (A) Chemical structures of the compounds. (B) c-Raf-1 coimmunoprecipitated with an anti-H-Ras antibody (top) and total c-Raf-1 (middle) and immunoprecipitated H-RasG12V (bottom) were detected in NIH3T3 cells transiently expressing H-RasG12V, which were treated with the 2 and 20 μM compound or DMSO in the presence of 2% FBS for 1 h. The numbers above the lanes show the values of H-Ras-bound/total c-Raf-1 relative to that of the vehicle-treated cells. (C) Phosphorylated MEK (pMEK) and ERK (pERK) as well as total MEK, ERK, and HA-tagged H-RasG12V were detected in NIH3T3 cells transiently expressing H-RasG12V, which were treated with 20 μM Kobe0065, 20 μM Kobe2602, or 2 μM sorafenib as described in (B). The numbers above

K-RasG12V. Rough estimates of the IC_{50} values for the cellular inhibition of Ras–Raf-binding are compatible with the K_i values for the *in vitro* inhibition considering a quite low cellular concentration of Raf. Consistent with this, the phosphorylation of downstream kinases MEK and ERK was effectively attenuated by 20 μM Kobe0065 and Kobe2602 in NIH3T3 cells transiently expressing H-RasG12V although their effect was a bit weaker than that of 2 μM sorafenib (Fig. 1.3C). On the other hand, the kinase activity of c-Raf-1 measured *in vitro* was not affected by the compounds [16], suggesting the absence of direct inhibitory activity toward Raf. Moreover, in the compound-treated cells, the levels of phosphorylated Akt and RalA·GTP were substantially reduced in a manner dependent on the compound concentrations (Fig. 1.3D), suggesting the inhibitory effects on the interaction of Ras with PI3Ks and RalGDS.

We next examined the effect of the compounds on Sos, which functions as not only an upstream regulator but also an effector of Ras. Sos has two distinct Ras-binding sites. One is the GEF domain that catalyzes GDP/GTP exchange on Ras through interaction with Ras·GDP and the other is the distal site that is located in close proximity to the GEF domain and allosterically accelerates its GEF catalytic activity through interaction with Ras·GTP [19]. *In vitro* GDP/GTP exchange assay using mSos1 and mSos1W729E, carrying an inactivating mutation of the distal site, showed that the accelerating effect of the distal site was almost completely abolished by 50 μM Kobe0065 without noticeably affecting the catalytic activity of the GEF domain (Fig. 1.3E), suggesting that the compound interferes with the interaction of Ras·GTP with the distal site but not of Ras·GDP with the GEF domain. The IC_{50} values for Kobe0065 and Kobe2602 were around 20 and 100 μM, respectively. This raised a possibility that the observed inhibition of the cellular function of H-RasG12V by the compounds might be accounted for by the decreased level of Ras·GTP due to the Sos inhibition. However, this possibility was effectively eliminated by our observation that the cellular RasG12V·GTP level remained

the lanes show the values of pMEK/tMEK and pERK/tERK relative to those of the vehicle-treated cells. (D) Phosphorylated Akt (pAKT) and RalA·GTP, pulled down with resin-immobilized Sec5 (residues 1–99), were detected at the same condition with (C). (E) Resin-immobilized H-Ras (residues 1–166)·GDP was incubated with [γ-^{35}S]GTPγS and purified mSos1(residues 563-1049), wild-type or a W729E mutant, at 25 °C in the presence or absence of 50 μM Kobe0065 and the radioactivity retained on the resin was measured. *Reproduced from Ref. [16].*

almost unaffected by either overexpression or siRNA-mediated knockdown of mSos1 in both NIH3T3 cells transiently expressing H-RasG12V and human colon cancer SW480 cells bearing K-RasG12V [16].

4.2. Inhibition of proliferation of cultured cancer cells

We examined the effects of the Kobe0065-family compounds on anchorage-dependent and -independent proliferation of cancer cells. The effect on anchorage-dependent cell proliferation at low serum condition was measured by using the MTT cell proliferation assay. The compounds at 20 μM almost completely inhibited the proliferation of H-*rasG12V*-transformed NIH3T3 cells in the presence of 2% fetal bovine serum (FBS) (Fig. 1.4A). The IC_{50} values were estimated to be approximately 1.5 and 2 μM for Kobe0065 and Kobe2602, respectively, which were a little higher than that (0.8 μM) for sorafenib. Further, apoptosis was frequently observed in the compound-treated cells (Fig. 1.4B), suggesting a contribution of the oncogene addiction mechanism to the antiproliferative effects of these compounds. The effects of the compounds on anchorage-independent proliferation of H-*rasG12V*-transformed NIH3T3 cells were examined by colony formation assays in 0.33% soft agar in the presence of 10% FBS. The compounds effectively inhibited colony formation in a dose-dependent manner (Fig. 1.5A). The estimated IC_{50} values for Kobe0065 and Kobe2602, 0.5 and 1.4 μM, respectively, were comparable to 2.1 μM for sorafenib. By contrast, the Kobe0065-family compounds were incapable of inhibiting the colony formation of anchorage-independent growth of NIH3T3 cells transformed by the activated c-*raf-1* gene carrying the S259A/Y340D/Y341D mutations, while sorafenib exhibited a potent inhibitory activity, further excluding their direct action on Raf. We then used several cancer cell lines with various oncogene mutations to assess the Ras specificity of the inhibition of anchorage-independent cell proliferation by the Kobe0065-family compounds (Fig. 1.5B). The compounds effectively inhibited the colony formation of cancer cells carrying the activated *ras* oncogenes irrespective of the *ras* isoforms and the nature of the mutations, such as colon cancer SW480 and pancreatic cancer PANC-1 (K-*rasG12V*), bladder cancer EJ-1 (H-*rasG12V*), fibrosarcoma HT1080 (N-*rasQ61L*), and colon cancer DLD-1 and HCT116 (H-*rasG13D*). By contrast, much weaker inhibition was observed in cancer cells without the *ras* mutation, such as A375, T-47D, LNCap, BxPC-3, MCF-7, HepG2,

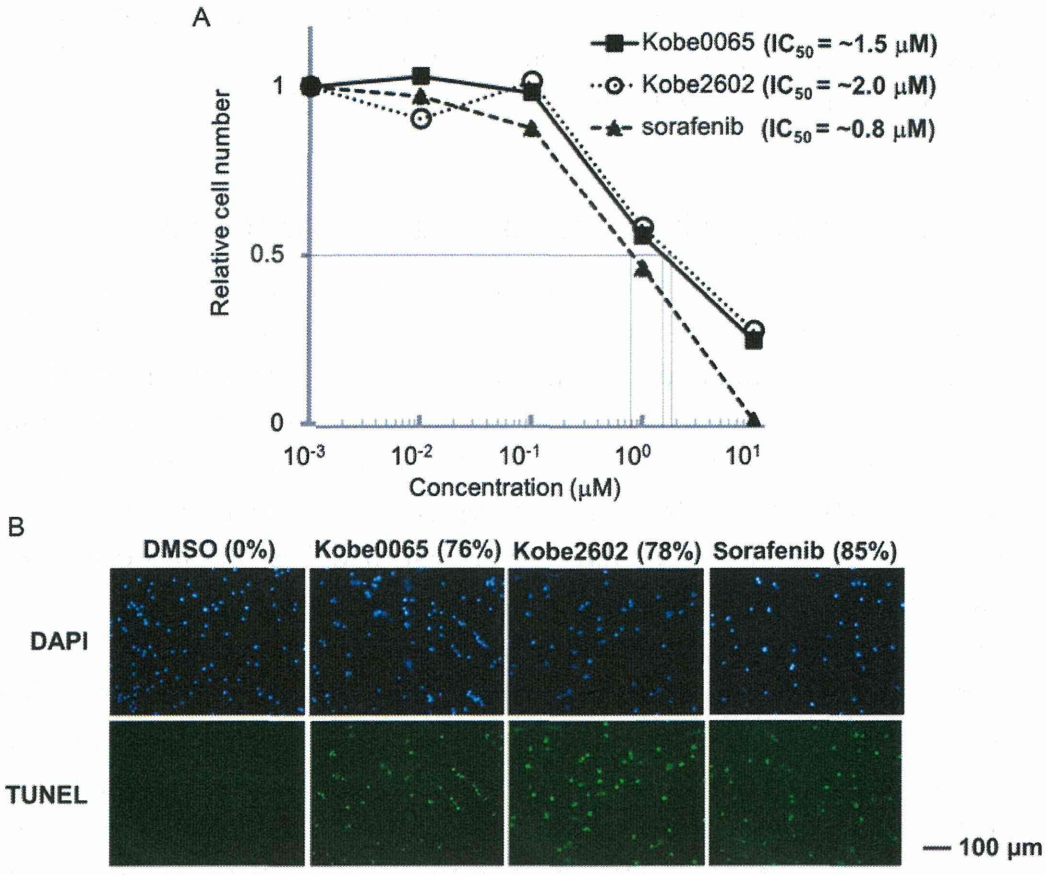

Figure 1.4 Inhibitory effects of the Kobe0065-family compounds on anchorage-dependent cell growth. (A) H-*rasG12V*-transformed NIH3T3 cells were treated with the 20 μM compound in the presence of 2% FBS for 72 h. Viable cell numbers were measured by the MTT cell proliferation assay. The IC_{50} values for Kobe0065, Kobe2602, and sorafenib were estimated from the corresponding dose–response curves. Each point represents the viable cell number at 72 h treatment relative to the initial number. (B) H-*rasG12V*-transformed NIH3T3 cells treated with the 20 μM compound in the presence of 2% FBS for 24 h were subjected to staining with 4′-6-diamidino-2-phenylindole (DAPI) (upper panels) and the TUNEL assay for detection of apoptotic cells (lower panels). The percentages show the ratio of the apoptotic cells among total cells. *Modified from Ref. [16].*

and HeLa. Both DLD-1 and HCT116 were sensitive to the compounds even though they carried additional activating mutations in PI3K, suggesting that the activated PI3K alone might be insufficient to sustain their anchorage-independent proliferation. This result is consistent with a recent report by Wang *et al.* [20], which showed that the interaction with K-RasG12V is necessary for the activated PI3K mutants to sustain proliferation of human breast cancer cells.